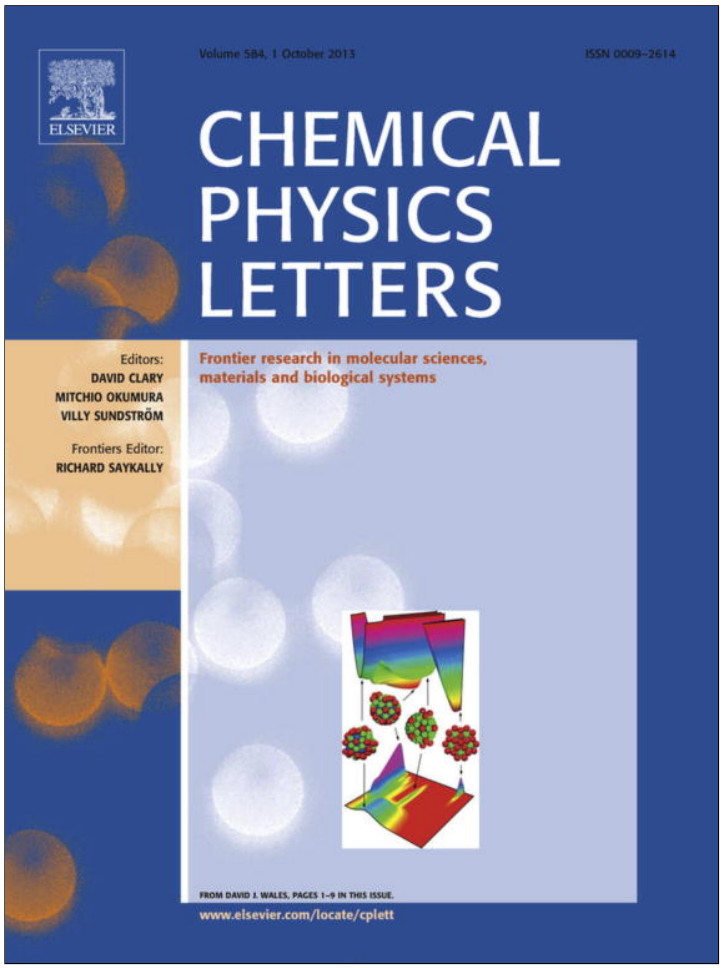

Chemical Physics Letters 584 (2013) 124–129

Contents lists available at ScienceDirect

Chemical Physics Letters

journal homepage: www.elsevier.com/locate/cplett

Hybrid graphene electrodes for supercapacitors of high energy density

Feifei Zhang [a,b,c], Jie Tang [a,b,*], Norio Shinya [a], Lu-Chang Qin [d,*]

[a] National Institute for Materials Science, Sengen 1-2-1, Tsukuba 305-0047, Japan
[b] Doctoral Program in Materials Science and Engineering, University of Tsukuba, 1-1-1 Tennodai, Tsukuba 305-8577, Japan
[c] Laboratory of Fiber Materials and Modern Textile, The Growing Base for State Key Laboratory, Qingdao University, Qingdao, Shandong 266071, China
[d] Department of Physics and Astronomy, University of North Carolina at Chapel Hill, Chapel Hill, NC 27599-3255, USA

ARTICLE INFO

Article history:
Received 9 July 2013
In final form 6 August 2013
Available online 14 August 2013

ABSTRACT

We describe a process of co-reduction to reduce dispersed graphene oxide (GO) and single-walled carbon nanotubes (SWNTs) simultaneously for preparation of hybrid electrodes for graphene supercapacitors. The SWNTs are in between the inter-layer space of graphene sheets as a spacer to prevent effectively restacking of graphene that often limits seriously the electrochemical performance of graphene supercapacitors. The SWNTs also act as conductive binders to improve the electrical conduction of the electrode. A high specific capacitance of 261 F g^{-1} for a single electrode and specific energy density of 123 W h kg^{-1} measured in the two-electrode configuration have been obtained in ionic liquid (EMI-TFSI).

1. Introduction

Supercapacitors have attracted significant attention recently due to their extraordinary high power density and long cycle life. They also bridge the power and energy gaps between traditional dielectric capacitors (which have high power output but low energy density) and batteries (which have high energy density but low power density). A major challenge for the development of supercapacitors has been to improve their energy density. Activated carbon (AC) has been the material of choice to fabricate the electrodes of supercapacitors for the past few decades [1–3]. However, AC-based supercapacitors have suffered a major setback that their energy density is still relatively low (typically 3–10 W h kg^{-1}) in comparison with best batteries which can offer energy density in the range 20–150 W h kg^{-1}.

With the discovery and availability of carbon nanotubes (CNTs) and especially graphene, a new opportunity has appeared to improve the energy density of supercapacitors drastically owing to the extraordinary physical, chemical, and electrochemical properties of these nanostructured carbon structures [4–8]. For example, graphene offers superior chemical stability, large specific surface area (~2630 m^2 g^{-1}), and a broad electrochemical window, which render it as a most attractive electrode material for supercapacitors with a theoretical electrochemical double layer capacitance of about 550 F g^{-1} [9].

Several interesting papers have been published during the past few years on utilizing graphene in supercapacitors. For example, Stoller et al. reported evaluation of supercapacitor electrodes made of a chemically modified graphene and specific capacitance of 135 F g^{-1} and 99 F g^{-1} was obtained in aqueous KOH and organic electrolyte, respectively [10]. Liu et al. reported a symmetric supercapacitor based on curved graphene nano-sheets which, when operated at a voltage of 4 V in an ionic liquid electrolyte, showed a high energy density of 85.6 W h kg^{-1} [11]. Very recently, El-Kady et al. used a standard LightScribe DVD optical drive to carry out reduction of graphite oxide films to produce graphene and the supercapacitor device made with the laser-reduced graphene exhibited high specific capacitance, ranging from 265 F g^{-1} in organic electrolyte operated at 3 V to 276 F g^{-1} in ionic liquid electrolyte operated at 4 V [12].

For high performance graphene supercapacitors, the desired key performance parameters for selected graphene are (i) high specific surface area, (ii) high intra- and inter-particle conductivity in porous graphene electrodes, and (iii) high electrolyte accessibility to the intra-pores in the graphene electrodes [13]. Among the various methods for preparation and processing of graphene, chemical reduction of graphene oxide is most promising owing to its low cost, easy operation, and scalability for mass production [14]. However, since the graphene nano-sheets tend to aggregate and restack through the van der Waals interactions during the reduction process, the effective specific surface area for access to the electrolyte is usually much lower than its theoretical value of 2630 m^2 g^{-1}. It is therefore of vital importance to prevent graphene from restacking in the process of fabrication of graphene electrodes. One idea is to use carbon nanotubes, especially single-walled carbon nanotubes, as spacers to prevent graphene from restacking and agglomerating. Attempts have been made to fabricate graphene electrodes with both multiwalled and single-walled carbon nanotubes and exciting results have been obtained with SWNTs [15–17]. As one can easily imagine, if CNTs could be inserted into the interlayer space of graphene nano-sheets, restacking of graphene can be

* Corresponding author. Fax: +1 9199620480.
E-mail address: lcqin@email.unc.edu (L.-C. Qin).

0009-2614/$ - see front matter © 2013 Elsevier B.V. All rights reserved.
http://dx.doi.org/10.1016/j.cplett.2013.08.021

prevented and, at the same time, the insertion of CNTs can also create certain intra-pores for the electrolyte to enter. In addition, due to the very high electrical conductivity of carbon nanotubes of 10^4 S m^{-1}, the internal electrical resistance of the graphene electrodes can also be reduced. As a result, we have recently developed a SWNT/graphene composite and the SWNT/graphene composite electrodes exhibited a specific capacitance of 201 F g^{-1} and high energy density of 63 W h kg^{-1} in organic electrolyte at room temperature [17].

In this Letter, to further improve the uniformity and electrochemical performance of the CNT/graphene composite, we report a co-reduction process, in which a suspension of graphene oxide (GO) and SWNTs is reduced simultaneously by hydrazine. As illustrated in Figure 1a, in the suspension the GO sheets are negatively charged when they are dispersed in water, as a result of ionization of the carboxylic acid and phenolic hydroxyl groups that are known to exist on the GO surface during oxidation of graphite. The GO suspension is colloidal [18,19]. The uniform SWNT suspension was obtained by non-covalent functionalization with sodium dodecyl benzene sulfonate (SDBS) molecules. SWNTs are dispersed as individual tubules and the amount of adsorption corresponds to coating of individual tubule surface with SDBS [20], and this process makes the surface of SWNTs become negatively charged (Figure 1b-1). Therefore, GO and SDBS-functionalized SWNTs can be well dispersed by electrostatic repulsions to form a dispersed suspension (Figure 1b-2). When this suspension is reduced by hydrazine, GO and SWNTs will deposit homogeneously, with which a uniform three-dimensional SWNT/graphene hybrid structure is obtained (Figure 1b-3). As the SWNTs are inserted into the interlayer space of graphene, buckling of otherwise flat graphene sheets will also likely occur and the restacking of graphene could therefore be effectively prevented. At the same time, intra-pores would be created to increase the specific surface area and the electrolyte ions would become more accessible to the electrode surface.

2. Experimental

2.1. Preparation of co-reduced SWNT/GO composites

Graphene oxide (GO) was synthesized from graphite by a modified Hummers–Offeman method [21]. Graphite and $NaNO_3$ powders were first mixed together in a beaker. H_2SO_4 was then added to the beaker with stirring in an ice water bath. $KMnO_4$ was added last to the suspension slowly to avoid overheating. The color of the suspension would eventually become brown and distilled water and H_2O_2 were then added and the color of the solution changed from brown to bright yellow. The final suspension was treated ultrasonically to exfoliate graphite oxide particles to produce graphene oxide platelets. Last refinement was carried out by centrifuge to remove larger particles. The final GO sediments were dried in a vacuum and the GO appears as dark brown powders with a typical size of about 10 μm. Atomic force microscopy (AFM) measurement indicated that the GO nano-sheet was a monolayer with a thickness of about 0.8 nm.

The finished GO powders were then dispersed in distilled water by sonication. SWNTs were added to a sodium dodecylbenzene sulfonate (SDBS) water solution or water to obtain an SWNT suspension. Then, the GO and SWNT suspensions were mixed and sonicated to produce a homogeneous suspension. Hydrazine hydrate was finally added into the suspension for reduction to obtain SWNT/GO(H_2O) and SWNT/GO(SDBS) composites.

2.2. Materials characterization

The morphologies and nanostructure of the graphene-based material were characterized using transmission electron microscopy (TEM, JEM-2100), scanning electron microscopy (SEM, JSM-7001F), and atomic force microscopy (AFM, Agilent's PicoScan). X-ray diffraction (XRD) was carried out using Rigaku RINT 2500 with Cu Kα radiation. Fourier transform infrared spectroscopy (FTIR) was recorded by SPECTRUM GX-Raman (Perkin Elmer). The specific surface area and pore size distribution were measured with Autosorb-1 (Quantachrome Instruments). All electrochemical characterization was performed using BioLogic EC-Lab (VSP-300).

2.3. Structure and evaluation of graphene supercapacitor

To compare the electrochemical performance of different graphene supercapacitors, graphene electrodes of almost the same weight of about 0.8 mg were prepared and assembled into coin cells using (i) pure SWNTs, (ii) hydrazine reduced graphene, and (iii) co-reduced SWNT/graphene composite. The electrode material

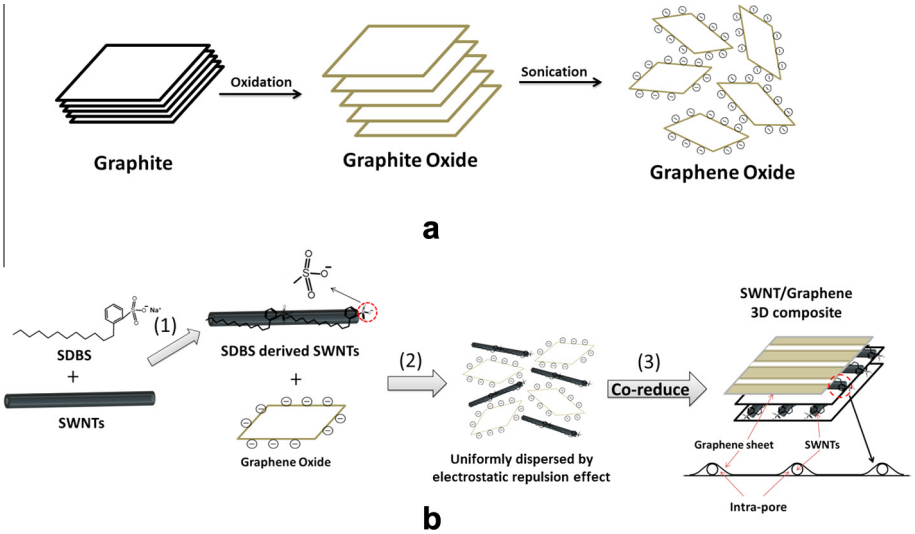

Figure 1. Schematic of chemical route for synthesis of graphene oxide and preparation of SWNT/graphene composite. (a) Oxidation of graphite to produce graphite oxide with greater interlayer spacing and exfoliation of graphite oxide in water by sonication to obtain GO colloids that is stabilized by electrostatic interactions. (b) Process of co-reduction of SWNT/GO to produce SWNT/graphene composite with SDBS surfactant.

was first dispersed separately in ethanol of concentration 0.2 mg ml^{-1} and then the suspension was filtered onto a porous filter membrane (Hydrophilic, 0.2 μm PTFE) by vacuum filtration. After vacuum drying at 25 °C for 24 h, all electrodes were prepared by cutting the filtered films into circular disks with diameter of 15 mm and a weight of about 0.8 mg for each electrode. Ionic liquid (1-ethyl-3-methylimidazolium-bis (trifluoromethylsulfonyl) imide, EMI-TFSI) was used as electrolyte in this Letter.

3. Results and discussion

Figure 2 shows the morphologies of co-reduced SWNT/GO composite. Figure 2a and b show the TEM and SEM images of co-reduced SWNT/GO composite with SWNTs pre-dispersed in H_2O (termed SWNT/GO(H_2O) hereafter). Since they do not disperse well in water, SWNTs often entangle to form bundles in the composite. We could also observe that graphene agglomerated, which made part of the graphene surface not accessible to the electrolyte. Figure 2c and d show the TEM and SEM images of co-reduced SWNT/GO composite with SWNTs pre-dispersed in water with 1% SDBS in solution (termed SWNT/GO(SDBS) hereafter). Negatively charged GO and SDBS functionalized SWNTs (also negatively charged) were well dispersed in suspension. In the structure the SWNTs were in between the graphene sheets resulting in a homogeneous SWNT/graphene composite. In addition, buckling of graphene also occurred because of the intra-pores created between the graphene layers.

Figure 3 shows the XRD patterns of (a) graphite oxide, (b) graphite, (c) hydrazine reduced graphene, (d) co-reduced SWNT/GO(H_2O), and (e) co-reduced SWNT/GO(SDBS). Graphite oxide showed a larger interlayer spacing (peak a, $2\theta = 11.3°$, $d = 0.78$ nm) than that of graphite ($d_{200} = 0.34$ nm). The increased spacing is because of the oxygen functional groups in graphite oxide and the water molecules held up in the interlayer spaces of the hydrophilic GO. In the XRD patterns of hydrazine reduced graphene and co-reduced SWNT/GO(H_2O) composite, the corresponding peak is at 24–25° due to an interlayer spacing of 0.35–0.37 nm. This spacing is much smaller than that of graphite oxide (0.78 nm), but closer to the (002) peak of graphite with $2\theta = 26.2°$ ($d = 0.34$ nm), indicating restacking of graphene nanosheets. On the other hand, in the case of co-reduced SWNT/GO(SDBS) composite, there is only a small broad peak appeared, suggesting that the GO powders were well dispersed with little restacking.

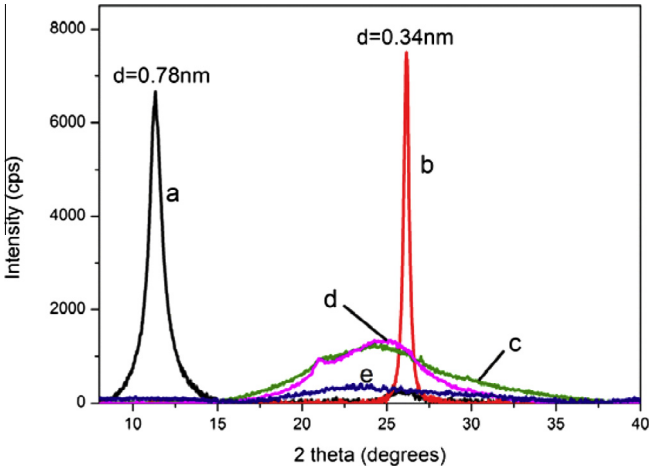

Figure 3. XRD patterns of different samples. (a) Graphite oxide; (b) Graphite; (c) Hydrazine reduced graphene; (d) Co-reduced SWNT/GO(H_2O); and (e) Co-reduced SWNT/GO(SDBS).

Nitrogen-adsorption and -desorption isotherms of SWNTs, hydrazine reduced graphene, and co-reduced SWNT/GO(SDBS) composite are shown in Figure 4a. Using these isotherms, the multipoint Brunauer–Emmett–Teller (BET) specific surface areas for SWNTs, hydrazine reduced graphene, and co-reduced SWNT/GO(SDBS) composite were obtained as 442.0, 587.3, and 945.6 $m^2 g^{-1}$. It should be noted that, the BET specific surface area

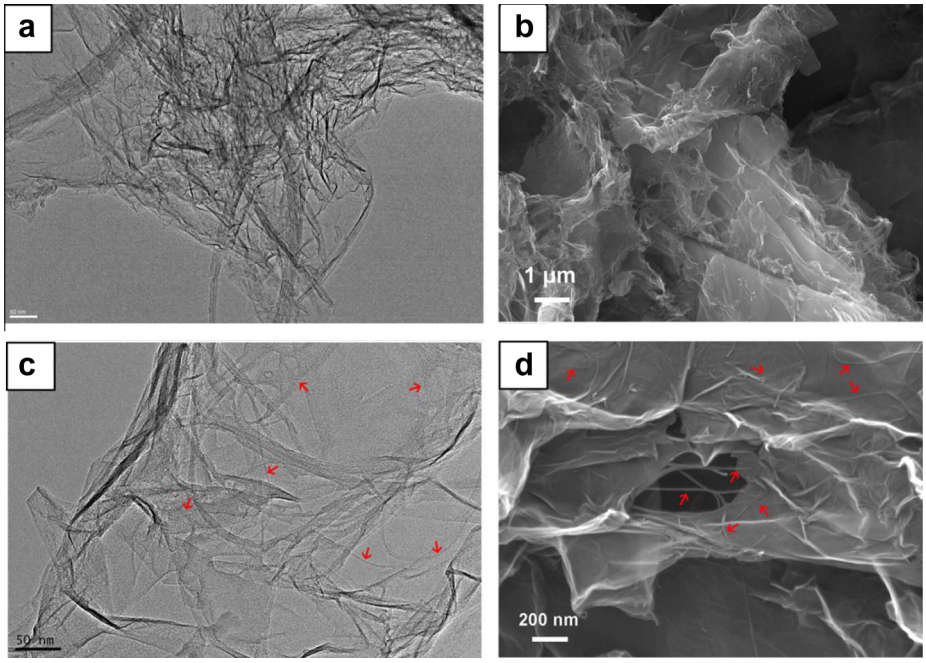

Figure 2. Morphology and structure of SWNT/graphene composite. (a) TEM and (b) SEM image of co-reduced SWNT/graphene composite with SWNTs dispersed in water. Few SWNTs were observed to have formed SWNT/graphene composite. (c) TEM and (d) SEM image of co-reduced SWNT/graphene composite with SWNTs dispersed with SDBS. SWNTs were well dispersed and homogeneous SWNT/graphene composite was obtained. The red arrows indicate SWNTs. (For interpretation of the references to colour in this figure legend, the reader is referred to the web version of this article.)

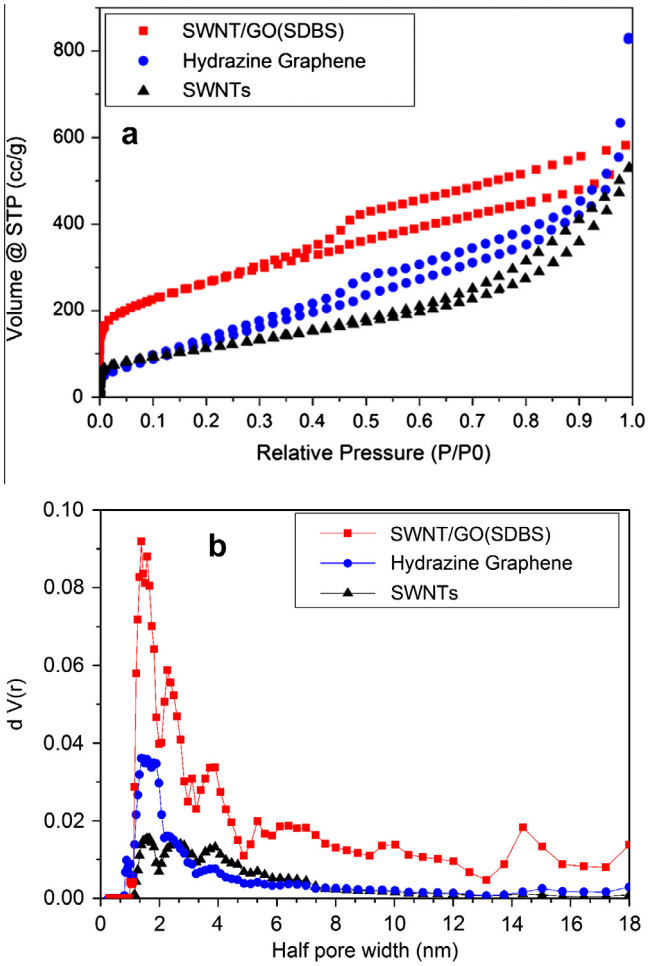

Figure 4. (a) Nitrogen adsorption and desorption isotherms and (b) pore size distribution of SWNTs (black), hydrazine reduced graphene (blue), and co-reduced SWNT/GO(SDBS) composite (red). (For interpretation of the references to colour in this figure legend, the reader is referred to the web version of this article.)

of the co-reduced SWNT/GO(SDBS) composite is much larger than that of SWNTs and hydrazine reduced graphene. This indicates that the dispersed SWNTs acted indeed as spacers between the graphene layers, thereby preventing their agglomeration and restacking, as revealed in Figure 2d. Based on the density functional theory (DFT) model, the pore size distribution of SWNTs, hydrazine reduced graphene, and co-reduced SWNT/GO(SDBS) composite is given in Figure 4b. The SWNT powders showed several wide peaks in the distribution, attributed to the SWNT bundles of various sizes. Pores from 1.4 to 2.0 nm in half width were observed in hydrazine graphene, which were due to graphene agglomeration. In the co-reduced SWNT/GO(SDBS) composite, there are three major pores with half width of 1.4, 2.3, and 3.8 nm. These data suggest that the SWNTs as spacers were inserted into the graphene layers, increasing the pore size and contributing to electrolyte accessibility and rate capability.

Figure 5 shows the Fourier transform infrared (FTIR) spectra of (a) GO, (b) hydrazine reduced graphene, (c) co-reduced SWNT/GO(H_2O) composite, and (d) co-reduced SWNT/GO(SDBS) composite. The GO sample shows a strong peak at 1597 cm^{-1} (skeletal vibrations from graphitic domains) due to the aromatic C=C bond. The peaks of GO at 1725 cm^{-1} (C=O stretching vibrations from carbonyl and carboxylic groups), 1425 cm^{-1} (C–O–C and C–OH stretching vibrations), 1256 cm^{-1} (epoxide groups), and 1060 cm^{-1} (C–O stretching vibrations), testify the presence of many oxygen-containing functional groups. In comparison to the

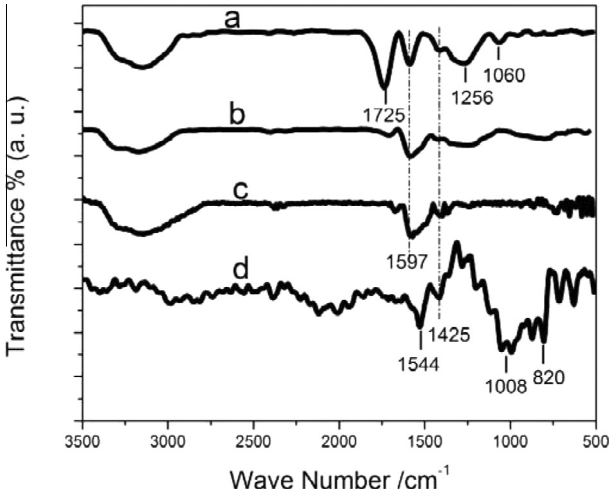

Figure 5. FTIR spectra of (a) GO; (b) Hydrazine reduced graphene; (c) Co-reduced SWNT/GO(H_2O) composite; and (d) Co-reduced SWNT/GO(SDBS) composite.

FTIR spectrum of GO, the peaks at 1725, 1256 and 1060 cm^{-1} in other samples almost diminished. This is because the C–O–C, C=O, and O–C=O were removed by hydrazine hydrate, which means GO and SWNT hybrid suspensions can be sufficiently reduced independent of the presence of SDBS. The peak at 1425 cm^{-1} did not disappear, indicating that most C–OH groups were still present and could not be reduced by hydrazine. The peaks in co-reduced SWNT/GO(SDBS) composite at about 1008 and 820 cm^{-1} are due to the remaining SDBS molecules.

Electrochemical characterization of the supercapacitor electrodes was performed using a symmetric two-electrode configuration with standard coin cells. The two-electrode test cell was used because it provides a most accurate measure of material performance for electrochemical capacitors [22].

Cyclic voltammetry (CV) curves were acquired at scanning rate from 10 to 100 mV s^{-1} and electrochemical impedance spectroscopy (EIS) was conducted using a sinusoidal signal with mean voltage of 0 and amplitude of 10 mV over a frequency range of 100 kHz to 10 mHz. The specific capacitance C_{sp}, energy density $E_{density}$, and power density $P_{density}$ were calculated from galvanostatic charge/discharge curves according to

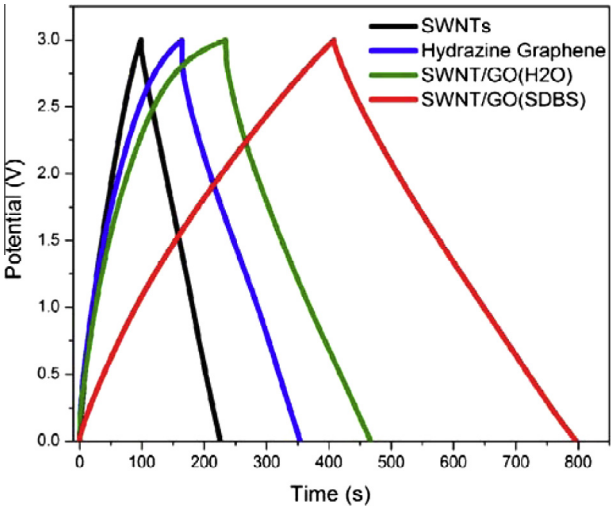

Figure 6. Galvanostatic charge/discharge curves up to 3.0 V of different electrodes at a constant current density of 320 mA g^{-1} in ionic liquid (EMI-TFSI) electrolyte.

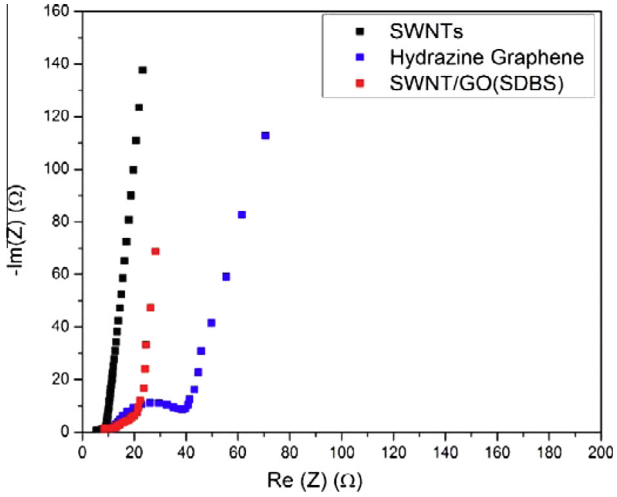

Figure 7. Nyquist plots of EIS data for SWNTs (black), hydrazine reduced graphene (blue), and co-reduced SWNT/GO(SDBS) (red) composite-based supercapacitors, using a sinusoidal signal with mean voltage of 0 V and amplitude of 10 mV over a frequency range of 100 kHz to 10 mHz. (For interpretation of the references to colour in this figure legend, the reader is referred to the web version of this article.)

$$C_{sp} = \frac{2I}{m(dV/dt)}, \tag{1}$$

$$E_{density} = \frac{1}{8} C_{sp} V_{drop}^2, \tag{2}$$

$$P_{density} = \frac{V_{drop}^2}{8mR_{ESR}}, \tag{3}$$

where dV/dt is calculated from the slope of the discharge curves, R_{ESR} is the equivalent series resistance, m is the weight of each electrode, and V_{drop} is the drop voltage.

Galvanostatic charge/discharge curves of symmetric supercapacitors based on pure SWNTs (black), hydrazine reduced graphene (blue), co-reduced SWNT/GO(H_2O) composite (green), and co-reduced SWNT/GO(SDBS) composite (red) at a constant current density of 320 mA g^{-1} in the potential range between 0 and 3 V are all shown in Figure 6.[1] It can be seen that the curves are nearly linear and symmetrical, showing typical and characteristic capacitive behavior. Only a very small voltage drop was observed, indicating that the electrodes had low internal resistance. In addition, the charge–discharge duration for co-reduced composites containing SWNTs was longer than that for hydrazine reduced graphene and pure SWNTs, indicating a higher specific capacitance. The increase in the specific capacitance of co-reduced composites is attributed to the functions of SWNTs acting as spacers for graphene layers to prevent restacking and therefore improving the accessibility for electrolyte ions. When compared the co-reduced SWNT/GO(H_2O) and SWNT/GO(SDBS) electrodes, the SWNT/GO(SDBS) electrodes exhibited higher specific capacitance and higher energy density, indicating that the uniformity of SWNT/graphene composites is crucial to the supercapacitor performance. In the co-reduced SWNT/GO(H_2O) electrode, there are still many restacked agglomerates of graphene and SWNT bundles and therefore the performance had limited improvement compared with pure graphene electrode. The specific capacitance and energy density obtained from galvanostatic charge/discharge curves for (i) SWNTs, (ii) hydrazine reduced graphene, (iii) co-reduced SWNT/GO(H_2O) composite, and (iv) co-reduced SWNT/GO(SDBS) composite, are 55, 86, 110, and 166 F g^{-1}. The corresponding energy densities are 17, 24, 26, and 50 W h kg^{-1}.

Figure 7 shows the Nyquist plots of the EIS data of supercapacitors with (i) pure SWNTs (black), (ii) hydrazine reduced graphene (blue), and (iii) co-reduced SWNT/GO(SDBS) (red) electrodes. The devices display nearly a pure capacitive behavior. A semicircle in the high frequency region and a straight line in the low frequency region are observed in all samples. The high

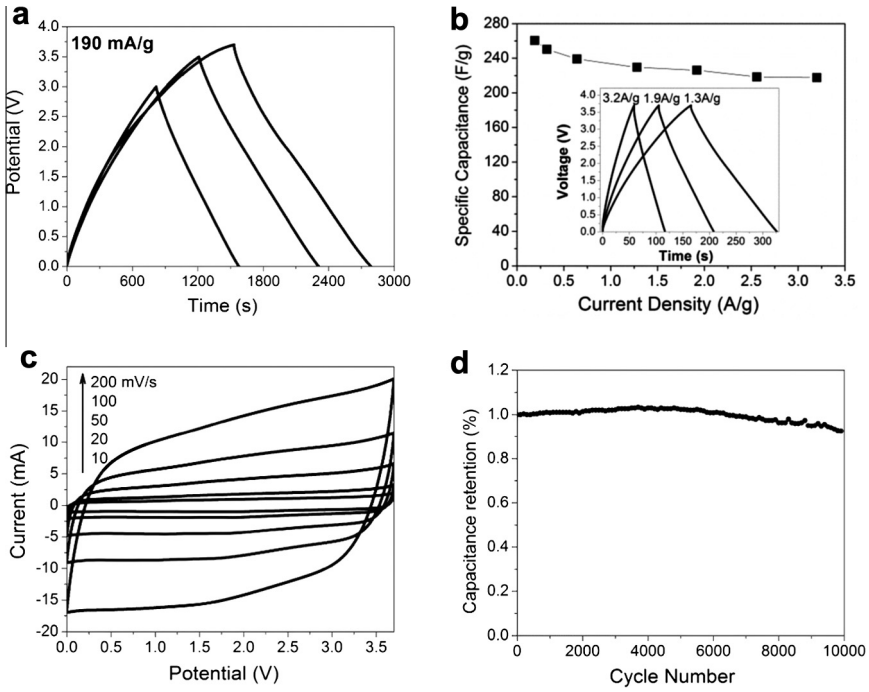

Figure 8. Evaluation of supercapacitor with co-reduced SWNT/GO(SDBS) composite electrodes. (a) Galvanostatic charge/discharge curves operated at current density of 190 mA g^{-1}, in the potential ranges of 0 to 3.0, 3.5 and 3.7 V. (b) Stack capacitance calculated from galvanostatic curves as a function of the charge/discharge current density (Inset is galvanostatic charge/discharge curves for SWNT/GO(SDBS) supercapacitor operated under different current density). (c) CV curves at scan rate of 10, 20, 50, 100, and 200 mV s^{-1}. (d) Cycling stability of the device in 10000 cycles.

frequency semicircle region has been observed in all carbon-based supercapacitors, which is related to the electric resistance within the electrode material. We can observe that the semicircle region for SWNTs is smaller than that for hydrazine reduced graphene, showing good conductivity of SWNTs. We can also find that the semicircle region for co-reduced SWNT/GO composite is smaller than that for hydrazine reduced graphene, indicating that the addition of SWNTs lowered the interlayer resistance of graphene sheets, therefore also acting as conductive binder. The magnitude of the equivalent series resistance (ESR) obtained from the intercept on the horizontal axis for SWNTs, hydrazine reduced graphene, and co-reduced SWNT/GO(SDBS) composite are 5.4, 8.5, and 10.6 Ω. The straight line in low frequency region of the co-reduced composite is shorter than that for SWNTs and graphene, indicating an enhanced access of electrolyte ions to the graphene surface, which is attributed to the insertion of SWNTs between graphene sheets.

We also tested the cyclic stability of the supercapacitor with SWNT/GO(SDBS) electrodes. The galvanostatic charge/discharge curves for the co-reduced SWNT/GO(SDBS) graphene supercapacitor at a constant current density of 190 mA g^{-1} in the potential ranges between 0 and 3.0, 3.5, and 3.7 V are shown in Figure 8a. The charge/discharge curves are nearly linear and symmetrical. The specific capacitance and energy density of the co-reduced SWNT/GO(SDBS) composite at current density of 190 mA g^{-1} and potential of 3.7 V are 261 F g^{-1}. The corresponding energy density and power density are 123 W h kg^{-1} and 255 kW kg^{-1}, respectively. The stack capacitance of a composite electrode is calculated from galvanostatic curves as a function of the applied charge/discharge current density is given in Figure 8b. This electrode shows a high rate capability as it continues to show high capacitance of 218 F g^{-1} even when the current density was increased to 3.2 A g^{-1}. The SWNT/GO(SDBS) composite retained 84% of its capacitance when the current density increased from 0.19 to 3.2 A g^{-1}.

The CV curves for the co-reduced SWNT/GO(SDBS) composite at different scan rate in the voltage range of 0–3.7 V are shown in Figure 8c. Even at the scan rate of 100 mV s^{-1}, the CV curve remained rectangular, indicating excellent capacitive characteristics. When the scan rate was increased to 200 mV s^{-1}, a CV curve with small oblique deformation was observed because of the relatively large resistance of ionic liquid electrolyte at high charging rate limited by ion diffusivity in the electrolyte. The stability of the co-reduced SWNT/GO(SDBS) graphene supercapacitor was also evaluated by conducting galvanostatic charge–discharge measurements for 10 000 cycles at a constant current of 2 m A in the potential range 1.0–3.7 V, which is shown in Figure 8d. The results indicate that the supercapacitor exhibited an excellent cycle life. There was no decay in capacitance observed in the first 5000 cycles. Even after 10 000 cycles, 94% of the electrode capacitance was retained, demonstrating long cycle life and stability.

4. Conclusions

A process of co-reduction has been established and demonstrated to produce SWNT/graphene composite with a three-dimensional network structure for applications in graphene supercapacitors. High specific capacitance of 261 F g^{-1} and energy density of 123 W h kg^{-1} have been obtained for the graphene supercapacitors at potential 3.7 V using ionic liquid electrolyte. We ascribe these improvements to (i) increase in the specific surface area of the co-reduced composite due to the spacer effect of SWNTs and that the resulted intra-pores offer better electrolyte accessibility to the graphene sheets and (ii) increase of electrical conductivity owing to the SWNT conductive binder. The SWNT/graphene supercapacitor of high specific capacitance and energy density would have promising applications in energy storage such as in hybrid vehicles and electrical vehicles.

Acknowledgements

This research was supported by the JST ALCA Program, JSPS and NSFC under the Japan–China Scientific Cooperation Program (21111140014), JSPS Grants-in-Aid for Scientific Research 22310074, and the Nanotechnology Network Project of the Ministry of Education, Culture, Sports, Science and Technology (MEXT), Japan.

References

[1] K. Kierzek, E. Frackowiak, G. Lota, G. Gryglewicz, J. Machnikowski, Electrochim. Acta 49 (2004) 1169.
[2] E. Raymundo-Pinero, K. Kierzek, J. Machnikowski, F. Beguin, Carbon 44 (2006) 2498.
[3] M. Endo, T. Maeda, T. Takeda, Y.J. Kim, K. Koshiba, H. Hara, M.S. Dresselhaus, J. Electrochem. Soc. 148 (2001) A910.
[4] B. Kim, H. Chung, W. Kim, Nanotechnology 23 (2012) 155401.
[5] M. Kaempgen, C.K. Chan, J. Ma, Y. Cui, G. Gruner, Nano Lett. 9 (2009) 1872.
[6] B. Xu, F. Wu, R.J. Chen, G.P. Cao, S. Chen, Z.M. Zhou, Y.S. Yang, Electrochem. Commun. 10 (2008) 795.
[7] A.K. Geim, K.S. Novoselov, Nat. Mater. 6 (2007) 183.
[8] S. Park, R.S. Ruoff, Nat. Nanotechnol. 4 (2009) 217.
[9] S. Vivekchand, C. Rout, K. Subrahmanyam, A. Govindaraj, C. Rao, J. Chem. Sci. 120 (2008) 9.
[10] M.D. Stoller, S.J. Park, Y.W. Zhu, J.H. An, R.S. Ruoff, Nano Lett. 8 (2008) 3498.
[11] C. Liu, Z. Yu, D. Neff, A. Zhamu, B.Z. Jang, Nano Lett. 10 (2010) 4863.
[12] M.F. El-Kady, V. Strong, S. Dubin, R.B. Kaner, Science 335 (2012) 1326.
[13] G. Wang, L. Zhang, J. Zhang, Chem. Soc. Rev. 41 (2012) 797.
[14] S. Stankovich, D.A. Dikin, R.D. Piner, K.A. Kohlhaas, A. Kleinhammes, Y. Jia, Y. Wu, S.T. Nguyen, R.S. Ruoff, Carbon 45 (2007) 1558.
[15] D. Yu, L. Dai, J. Phys. Chem. Lett. 1 (2009) 467.
[16] Y.S. Kim, K. Kumar, F.T. Fisher, E.H. Yang, Nanotechnology 23 (2012) 015301.
[17] Q. Cheng, J. Tang, J. Ma, H. Zhang, N. Shinya, L.-C. Qin, Phys. Chem. Chem. Phys. 13 (2011) 17615.
[18] A. Lerf, H. He, M. Forster, J. Klinowski, J. Phys. Chem. B 102 (1998) 4477.
[19] T. Szabó, O. Berkesi, P. Forgó, K. Josepovits, Y. Sanakis, D. Petridis, I. Dékány, Chem. Mater. 18 (2006) 2740.
[20] S. Utsumi, M. Kanamaru, H. Honda, H. Kanoh, H. Tanaka, T. Ohkubo, H. Sakai, M. Abe, K. Kaneko, J. Colloid Interface Sci. 308 (2007) 276.
[21] W.S. Hummers, R.E. Offeman, J. Am. Chem. Soc. 80 (1958) 1339.
[22] M.D. Stoller, R.S. Ruoff, Environ. Sci. 3 (2010) 1294.